From Bubbles to Clusters in Fluidized Beds

B. J. Glasser
Department of Chemical and Biochemical Engineering, Rutgers University, Piscataway, New Jersey 08854

S. Sundaresan and I. G. Kevrekidis
Department of Chemical Engineering, Princeton University, Princeton, New Jersey 08544
(Received 30 January 1998; revised manuscript received 4 June 1998)

Clusterlike solutions are reported for volume-averaged equations of motion in fluidized gas-particle suspensions (i.e., fluidized beds). A connection between bubbles and clusters is established through bifurcation analysis and numerical continuation in the mean volume fraction of the suspension. The robustness of this connection is established by varying the model parameters and the closures. The bubbles and clusters are shown to belong to the same family of nonuniform solutions. [S0031-9007(98)06999-3]

PACS numbers: 47.55.Kf, 46.10.+z, 47.55.Dz

Granular materials in general, and fluidized suspensions of them in particular, are encountered in a variety of industries [1,2]. In many applications it is important that the grains are continuously moving as this allows for mixing, and heat or mass transfer between the solids and a fluid phase. Yet granular materials will come to rest (as a result of gravity and the dissipative nature of collisions) unless "energy" is continuously fed into the system [1,2]. Sources of energy include movement of the confining walls or internals (e.g., stirring, mixing, vibration, or rotation) and flow of a fluid through the voids between the particles (e.g., a fluidized bed). To fluidize a bed of particles in a vertical cylinder, a fluid (a gas) is passed upwards through a distributor on which the particles rest. When the flow rate is sufficiently large that the available pressure drop across the bed is able to support its weight, the particles become mobile and the bed is said to be fluidized. As the flow rate of the gas is further increased, the bed of particles may expand smoothly such that the mean volume fraction of solids is uniform throughout the bed [2]. Such a uniformly fluidized bed is rarely realized in practice. Instead, concentration waves move upwards through the bed and take the form of compact regions of low particle concentration (bubbles), alternating bands of high and low particle concentration (slugs) as well as compact regions of high particle concentration (clusters) [2–7]. These significantly affect the dynamics of the bed.

As discussed by Daw *et al.* [8], length scales of the bulk or macroscopic motion are typically 3 orders of magnitude larger than the length scales of individual particle or microscopic motion. Yet, such macroscopic behavior requires the collective and organized motion of many particles. Such collective particle behavior is not restricted to fluidized beds; bubbling has also been observed in vertically vibrated granular materials [9], and clustering has been observed in simulations of sheared and unforced granular materials [10]. Thus, an understanding of the origin of such structures and the minimum physics needed to capture their occurrence is of fundamental importance. Using a bifurcation analysis we have followed the solution structure of volume-averaged (macroscopic) equations of motion describing fluidized beds, and found that by varying parameters of the system we could move smoothly between the seemingly different structures observed in fluidized beds, namely slugs, bubbles, and clusters.

Volume-averaged equations have been described extensively in the literature (e.g., Ref. [5]). We analyze volume-averaged equations of motion [11] for the (incompressible) fluid and particle phases of a fluid-particle suspension

$$\rho_s \phi \frac{D\mathbf{u}_s}{Dt} = -\nabla \cdot \boldsymbol{\sigma}_s - \phi \nabla \cdot \boldsymbol{\sigma}_f + k\tilde{\mathbf{f}} + \phi \rho_s \mathbf{g}, \quad (1)$$

$$\rho_f (1-\phi) \frac{D\mathbf{u}_f}{Dt} = -(1-\phi)\nabla \cdot \boldsymbol{\sigma}_f - k\tilde{\mathbf{f}} + (1-\phi)\rho_f \mathbf{g}, \quad (2)$$

where D/Dt is the material derivative, $\mathbf{u}_s$ and $\mathbf{u}_f$ are the solids and fluid velocities, respectively, ϕ is the volume fraction of solids, $\boldsymbol{\sigma}_s$ and $\boldsymbol{\sigma}_f$ are the solid and fluid phase stress tensors (defined in a compressive sense), respectively, k is the number of particles per unit volume, $\tilde{\mathbf{f}}$ is the average force exerted on a particle by the fluid due to the relative motion between the phases, and $\mathbf{g}$ is the gravity force vector. These quite general equations of motion, along with continuity equations, must be closed through constitutive relations; here we employ the closures of Ref. [12], originally motivated by Refs. [5,11]. While one may argue about the validity of any constitutive relations for gas-particle suspensions, we have adopted what we believe are the simplest credible constitutive relations that can describe a fluidized bed. We will show that our model equations contain the necessary physics to capture the flow regimes of interest in a gas-fluidized bed.

The stress tensors, as proposed in Ref. [11], are assumed to obey the following form:

$$\boldsymbol{\sigma}_i = p_i \mathbf{I} - \mu_i \left[\nabla \mathbf{u}_i + (\nabla \mathbf{u}_i)^T - \frac{2}{3}(\nabla \cdot \mathbf{u}_i)\mathbf{I} \right],$$

where $\{i = s, f\}$ for the solids and fluid, respectively; μ refers to viscosity, and p to pressure. The particle phase pressure, of the form [12]: $p_s = C\phi/(\phi_p - \phi)^2$, increases from zero ($\phi = 0$) and diverges as the solids fraction tends to the random close-packed value, ϕ_p. In the case of gas-fluidized beds the interaction force $\tilde{\mathbf{f}}$ arises primarily because of interphase drag. The interphase drag force per unit volume is given by the bed expansion measurements of Richardson and Zaki [13] where

$$k\tilde{\mathbf{f}} = \frac{\phi(\rho_s - \rho_f)g}{v_t(1 - \phi)^{(n-2)}}[\mathbf{u}_f - \mathbf{u}_s].$$

The exponent n is a function of the particle Reynolds number, $R_t = 2av_t\rho_f/\mu_f$; v_t is the terminal velocity of a particle of radius a. The equations were cast in a dimensionless form using ρ_s, v_t, $L = (\mu_s v_t/\rho_s g)^{1/2}$, and $T = L/v_t$ as characteristic density, velocity, length, and time, respectively [12].

We analyze the solution structure for two-dimensional beds of infinite extent, seeking spatially periodic solutions. 200 μm diameter glass beads fluidized by air at ambient conditions were chosen as the base case due to abundant experimental work on this system [12]. The base parameter values, in the right range suggested by experiments, were chosen as [12] $a = 100$ μm, $\rho_s = 2200$ kg/m^3, $\mu_s = 0.665$ kg/ms, $C = 0.0388$ Pa, $v_t = 1.423$ m/s, $n = 4.35$, $\phi_p = 0.65$.

An equilibrium solution to the closed equations of motion and continuity is a uniform fluidized bed of infinite extent, $\phi = \phi_0$; $\mathbf{u}_s = \mathbf{0}$; $\mathbf{u}_f = \mathbf{j}u_0$, where $\mathbf{j}$ is the unit vector in the y direction, which is pointing vertically upward, and ϕ_0 and u_0 are constants. The linear stability of this solution against small, spatially periodic one- and two-dimensional disturbances has been examined by many researchers (e.g., Refs. [5,6,12]). When ϕ_0 (the mean volume fraction in the bed) lies between a critical lower value and a critical upper value, the state of uniform fluidization is linearly unstable and the fastest growing disturbance is a traveling wave with no horizontal structure (a one-dimensional traveling wave, 1D-TW). The wave takes the form of alternating bands of high and low voidage, which move upwards through the bed. In dense beds (high ϕ_0) such waves resemble "slugs" in fluidized beds [5,14]. We will show that such waves also exist for dilute beds (low ϕ_0) and can be traced continuously from the dense to the dilute end.

Every 1D-TW is characterized by two parameters, namely ϕ_0 and k_y (the vertical wave number), and has its own wave speed, c with respect to the laboratory frame (the frame of reference where the average flux of particles in the periodic box is zero). In a frame of reference moving at c the wave will appear steady. We study, computationally, families of traveling waves generated by allowing ϕ_0 to vary at constant k_y; they arise at Hopf bifurcation points. The Fourier series based discretization and bifurcation-continuation procedure are discussed in Ref. [12].

Figure 1a shows the particle volume fraction norm, $\|A_\phi\|$ (the L_2 norm of the Fourier coefficients for the particle volume fraction) as a function of ϕ_0 for various k_y values. $\|A_\phi\|$ gives a measure of the amplitude of the solution relative to the base uniform state (the line $\|A_\phi\| = 0$). We will first focus on the branch of solutions obtained for $k_y = 0.33$ [curve (i) in Fig. 1a]. At point A there is a Hopf bifurcation and the uniform state becomes unstable to disturbances with vertical wave numbers of 0.33. The branch terminates at the uniform state in another Hopf bifurcation at point J.

Plots of ϕ versus scaled height, Y^* ($= Yk_y/2\pi$), in the traveling wave frame for the 1D-TW's corresponding to points P to U in Fig. 1a are shown in Fig. 1b. Traversing the 1D-TW branch from point A, the waves start with small amplitude and are nearly sinusoidal. As the mean volume fraction of solids increases, the waves increase in amplitude and become asymmetric with a fairly flat low ϕ region (curve P in Fig. 1b); the wave amplitude continues to increase and at higher ϕ_0 (curve Q) a localized region of high volume fraction develops, surrounded by a flat region of low volume fraction. The extent of this localized high ϕ region subsequently grows in size (relative to the low ϕ region) as shown in curves R and S.

Past point S in Fig. 1a the waves start to change in structure, and at point T the "inverse" structure (a localized region of low ϕ surrounded by a fairly flat region of high ϕ) develops. Further along the diagram, after a turning point in ϕ_0 (just before point U) the branch eventually terminates at the base state (point J in Fig. 1a). Solutions close to the base state are again sinusoidal in shape. The solution structures of 1D-TW branches for other k_y values are similar to that shown in Fig. 1b. However, as k_y is increased (decreased) the amplitude of the solutions decreases (increases) for a given ϕ_0.

The waves, extended periodically, represent alternating bands of high and low volume fraction which propagate upwards through the bed. A heuristic argument for propagation of the waves can be obtained by focusing on the solids rich bands. The lower surface of each solids rich band is "unstable" and particles rain down from

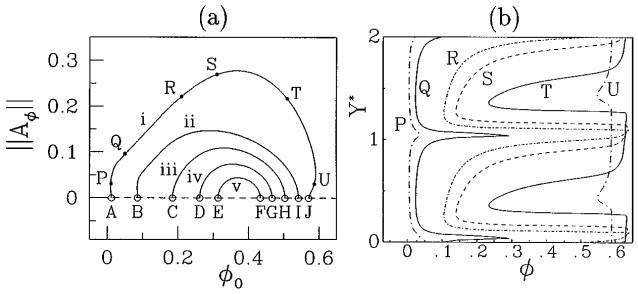

FIG. 1. (a) Amplitude of 1D-TW solutions, $\|A_\phi\|$, versus ϕ_0 for different vertical wave numbers, k_y. (i) $k_y = 0.33$, (ii) $k_y = 0.66$, (iii) $k_y = 4.64$, (iv) $k_y = 5.30$, (iv) $k_y = 5.64$. ∘-Hopf bifurcation point. (b) Plot of ϕ versus dimensionless height showing 1D-TW solutions (over two spatial periods, for clarity) corresponding to points P to U in Fig. 1a.

it; they accelerate under gravity and their concentration decreases on moving down (leading to the formation of the band of low particle concentration). The particles then decelerate rapidly as they meet the upper boundary of the solids rich band below. This transfer of the particles from each solids rich band to its neighbor below leads to the upwards motion of the whole concentration pattern.

We analyzed the linear stability of the 1D-TW's shown in Fig. 1b against transverse (lateral, x direction) disturbances. Figure 2 shows results for the $k_y = 4.64$, 1D-TW branch, labeled $CKVOH$, and a fixed lateral wave number of $k_x = 3.61$. The 1D-TW branch starting at C is initially stable as ϕ_0 increases. At point K it loses stability to a new branch of two-dimensional solutions, still traveling vertically up through the bed at constant wave speeds (two-dimensional vertical traveling waves or 2D-TW's). This is a pitchfork bifurcation in the moving frame: one real eigenvalue goes through zero at K. The 2D-TW branch ($KLMNO$) goes through a maximum and then returns to the 1D-TW branch at point O (another pitchfork bifurcation). As k_x is increased the 1D-TW branch loses stability at higher amplitude and the bifurcation points change location (they move up the branch). For large enough k_x they come together in a codimension two bifurcation and the 1D-TW is linearly stable to lateral disturbances. Thus the loss of stability of the 1D-TW's in the lateral direction is a long wave instability and one-dimensional waves are stable (and so observable) for large k_x, corresponding to narrow tubes. Indeed, the familiar "slugging" behavior is observed in narrow tubes.

Every fully developed 2D-TW is characterized by three parameters, namely ϕ_0, k_y, and k_x. We have examined a large variety of combinations of parameters for which 2D-TW's exist. The basic solution structure shown in Fig. 2 was observed for all the combinations we examined. One-dimensional traveling waves emerge through a Hopf bifurcation of the uniform state, and two-dimensional traveling waves are born from these in a secondary instability.

We traced the 2D-TW's smoothly from the dense to the dilute end, and a gallery of representative solutions is presented in Figs. 3a–3j. The corresponding parameter values for these solutions are reported in the caption; these values are somewhat arbitrary. Six equally spaced voidage contours (white corresponding to the minimum and black to the maximum ϕ value of each image) are plotted for an entire periodic box (dimensionless width $2\pi/k_x$ and height $2\pi/k_y$). 1D-TW's at low and high ϕ_0 are included for reference in Figs. 3a and 3j, respectively. 2D-TW's close to their onset exhibit bulging (Fig. 3b) or buckling of the 1D-TW structure.

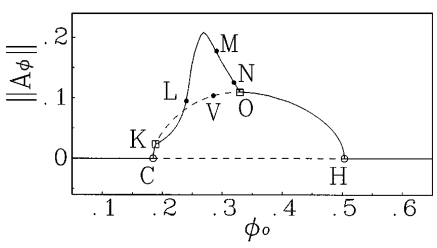

FIG. 2. Plot of $\|A_\phi\|$ versus ϕ_0 showing the 1D-TW and 2D-TW branches. $k_y = 4.64$, $k_x = 3.61$.

At the dilute end for $k_x > k_y$ clusterlike solutions are observed: localized regions of high volume fraction surrounded by a nearly flat region of low volume fraction of solids (Fig. 3c). As k_x approaches k_y, the flat region of low volume fraction starts to gain structure and a column-like solution begins to develop (Fig. 3d). This type of solution becomes more apparent as the ratio of k_y/k_x is further increased (Fig. 3e). Similar structures have been seen experimentally and are commonly referred to as "streamers" [2]. As ϕ_0 is increased the localized region of high solids fractions grows in size (analogous to 1D-TW observations above). In Fig. 3f we present a solution where the region of high volume fraction is no longer

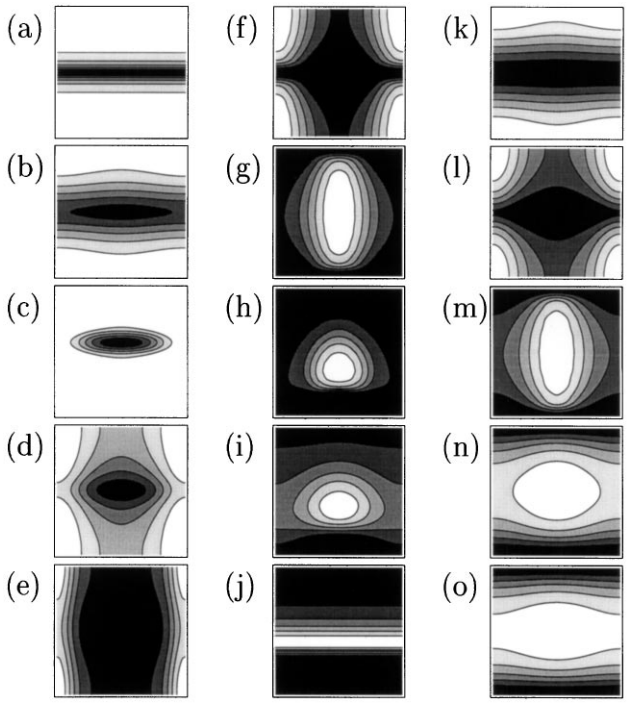

FIG. 3. Representative contour plots of ϕ. Plots (k) to (o) are 2D-TW's corresponding to points close to the locations labeled K to O in Fig. 2. The maximum and minimum ϕ values are given for each contour plot. (a) $\phi_0 = 0.011$, $k_y = 0.3$, $k_x = 0$, $0.006 < \phi < 0.04$, (b) $\phi_0 = 0.02$, $k_y = 0.6$, $k_x = 4.0$, $0.016 < \phi < 0.028$, (c) $\phi_0 = 0.03$, $k_y = 0.2$, $k_x = 4.3$, $0.02 < \phi < 0.14$, (d) $\phi_0 = 0.045$, $k_y = 0.6$, $k_x = 3.3$, $0.009 < \phi < 0.11$, (e) $\phi_0 = 0.06$, $k_y = 0.8$, $k_x = 0.8$, $0.05 < \phi < 0.07$, (f), (g) $\phi_0 = 0.345$, $k_y = 4.6$, $k_x = 2.9$, $0.07 < \phi < 0.52$, (h) $\phi_0 = 0.56$, $k_y = 1.2$, $k_x = 1.2$, $0.31 < \phi < 0.63$, (i) $\phi_0 = 0.57$, $k_y = 1.4$, $k_x = 1.4$, $0.47 < \phi < 0.61$, (j) $\phi_0 = 0.58$, $k_y = 0.33$, $k_x = 0$, $0.55 < \phi < 0.59$. For (k) to (o): $k_y = 4.64$, $k_x = 3.61$. (k) $\phi_0 = 0.19$, $0.17 < \phi < 0.22$, (l) $\phi_0 = 0.24$, $0.11 < \phi < 0.32$, (m) $\phi_0 = 0.29$, $0.06 < \phi < 0.46$, (n) $\phi_0 = 0.326$, $0.22 < \phi < 0.49$, (o) $\phi_0 = 0.329$, $0.24 < \phi < 0.49$.

localized: it bridges (both vertically and laterally) the domain edges, and (due to the periodic BC's) the entire column. Figure 3g is a shift (laterally by π/k_x and vertically by π/k_y) of the solution in Fig. 3f. A localized, low volume-fraction region is highlighted (Fig. 3g), and becomes more localized at smaller mean volume fractions (Fig. 3h). Such bubblelike solutions are discussed in detail elsewhere [12]; they remarkably resemble experimentally observed bubbles in fluidized beds possessing, among other salient features, their hemispherical shape. This is noteworthy, considering the simplicity of the model. 2D-TW's close to the 1D-TW branch at the dense end exhibit a buckling (Fig. 3i) or a bulging (Fig. 3o) type structure. The exact amplitude, steepness, and shape of the solution will depend on the values of the three parameters ϕ_0, k_y and k_x. Figures 3k–3o demonstrate the gradual qualitative change in the 2D solution contours for fixed k_x and k_y with increasing particle volume fraction along the one-parameter diagram of Fig. 2.

The robustness of the solution structure was examined through different model parameters, gas-particle systems, different closures for the interphase drag, the solids phase pressure, and a solids viscosity which varies with solids fraction [12]. The same basic hierarchy of solutions (described above) was observed. The subcritical-supercritical nature of the branches and the exact shape of the solutions is dictated by the parameter values and form of the closures; however, the basic topology of the bifurcation diagram with respect to volume fraction, and the gradual transformation of the fully developed solution structures between the dense and dilute ends of this diagram, remain the same. A technical problem arises when the low density instability is pushed to $\phi = 0$ for a certain class of particle pressure closures (those with $p_s \sim \phi^\alpha$ as $\phi \to 0$, with $\alpha > 1$). While we cannot trace branches from such a degenerate (and unphysical) critical point, we believe that one can still trace fully developed nonlinear solutions through continuation in ϕ_0 from the dense end.

The propagation of the 2D-TW's is analogous to that of the 1D-TW's, but it now involves both vertical and lateral movement of material. However, in the laboratory frame of reference this lateral movement is relatively small. This is not surprising since the motion of the wave is purely vertical. The lower surfaces of solids rich regions are unstable and solids accelerate under gravity and rain down into the low solids fraction regions. The particles will then decelerate rapidly if they meet another solids rich region. The particles will thus rain down from the lower surface of a solids rich region and collect on the upper surface of a solids rich region. This same mechanism leads to propagation of a bubblelike structure or a clusterlike structure.

Our results show that whether an instability of the uniform state leads to a cluster or a bubble is based on which "phase" (high solids or low solids) is continuous. In a dense bed the region of high solids fraction is continuous and thus bubbles are observed. In the dilute beds the converse is true. In beds of intermediate mean solids fraction the structures that form are "intermediate" in nature, in between bubbles and clusters. Thus even though a bubble and a cluster look very different in a fluidized bed, our results suggest that they both form and propagate by the same mechanism; in a sense they are one and the same.

These results are qualitative in nature due to uncertainties in the necessary model closures. At the same time this work shows that the phenomenon of interest is not dependent on the details of the closures. In the dilute gas-solid systems considered here, cluster formation involves an interplay of gravity, particle phase stress, drag, and inertia. In contrast, in dissipative granular gases, clusters arise due to an inelastic collision mechanism [10] which is not treated in our analysis. In general, both mechanisms can operate and lead to clusters in gas-solid suspensions.

The computational work was carried out through a grant of time on a CRAY C90 from the Pittsburgh Supercomputing Center. We are grateful to Professor Roy Jackson for his help and advice over the course of this work and to the National Science Foundation and the Exxon Education Foundation for partial support.

[1] H. M. Jaeger and S. R. Nagel, Science **255**, 1523 (1992).
[2] D. Kunii and O. Levenspiel, *Fluidization Engineering* (Butterworth, London, 1991), 2nd ed.
[3] M. M. El-Kaissy and G. M. Homsy, Int. J. Multiphase Flow **2**, 379 (1976); G. M. Homsy, M. M. El-Kaissy, and A. K. Didwania, Int. J. Multiphase Flow **6**, 305 (1980); J. M. Ham *et al.*, Int. J. Multiphase Flow **16**, 171 (1990).
[4] M. Nicolas *et al.*, Phys. Fluids **8**, 1967 (1996).
[5] R. Jackson, in *Fluidization*, edited by J. F. Davidson, R. Clift, and D. Harrison (Academic, London, 1985).
[6] M. F. Göz, J. Fluid Mech. **303**, 55 (1995); S. E. Harris and D. G. Crighton, J. Fluid. Mech. **266**, 243 (1994).
[7] J. R. Grace and J. Tuot, Trans. Inst. Chem. Eng. **57**, 49 (1979).
[8] C. S. Daw *et al.*, Phys. Rev. Lett. **75**, 2308 (1995).
[9] H. K. Pak and R. P. Behringer, Nature (London) **371**, 231 (1994).
[10] I. Goldhirsch and G. Zanetti, Phys. Rev. Lett. **70**, 1619 (1993); M. A. Hopkins and M. Y. Louge, Phys. Fluids A **3**, 47 (1991).
[11] T. B. Anderson and R. Jackson, I&EC Fund. **6**, 527 (1967); **7**, 12 (1968).
[12] B. J. Glasser, Ph.D. thesis, Princeton University, 1996; B. J. Glasser, I. G. Kevrekidis, and S. Sundaresan, J. Fluid Mech. **306**, 183 (1996).
[13] J. F. Richardson and W. N. Zaki, Trans. Inst. Chem. Eng. **32**, 35 (1954).
[14] See K. G. Anderson, S. Sundaresan, and R. Jackson, J. Fluid Mech. **303**, 327 (1995), and references therein.